

Article

Trimetallic ($\text{Au}_{\text{rod}}\text{-Pd}_{\text{shell}}\text{-Pt}_{\text{cluster}}$) Catalyst Used as Amperometric Hydrogen Peroxide Sensor

Shou-I Cheng ^{1,†}, John Rick ^{1,†}, Chun-Jern Pan ¹, Hung-Lung Chou ², Wei-Nien Su ², Kuan-Jung Chen ¹, Chung-Chiun Liu ³, Yaw-Wen Yang ⁴, Chia-Hsin Wang ⁴ and Bing-Joe Hwang ^{1,4,*}

¹ Nanoelectrochemistry Laboratory, Department of Chemical Engineering, National Taiwan University of Science and Technology, Taipei 106, Taiwan; E-Mails: asoonas2009@yahoo.com.tw (S.-I.C.); nouveavous@yahoo.com (J.R.); pom9106054@yahoo.com.tw (C.-J.P.); d9706002@mail.ntust.edu.tw (K.-J.C.)

² Graduate Institute of Applied Science and Technology, National Taiwan University of Science and Technology, Taipei 106, Taiwan; E-Mails: a8406033@mail.ntust.edu.tw (H.-L.C.); wsu@mail.ntust.edu.tw (W.-N.S.)

³ Department of Chemical Engineering, Case Western Reserve University, Cleveland, OH 44106, USA; E-Mail: cxl9@case.edu

⁴ National Synchrotron Radiation Research Center, Hsinchu 30076, Taiwan; E-Mails: yang@nsrrc.org.tw (Y.-W.Y.); wang.ch@nsrrc.org.tw (C.-H.W.)

† These authors contributed equally to this work.

* Author to whom correspondence should be addressed; E-Mail: bjh@mail.ntust.edu.tw; Tel.: +886-2-2733-3141 (ext. 6624); Fax: +886-2-2737-6922.

External Editor: Jeff D. Newman

Received: 2 July 2014; in revised form: 8 September 2014 / Accepted: 16 September 2014 /

Published: 19 November 2014

Abstract: Bimetallic nanostructured core-shell structures are commonly used as catalysts in a wide variety of reactions. We surmised that the addition of an additional metal would potentially allow catalytic tailoring with the possibility of an increase in activity. Here a tri-metallic catalytic structure, consisting of clustered catalytic Pt on the surface of a Pd shell supported on a rod shaped Au core was fabricated. The significance of the additional metallic component is shown by comparative electrochemically active surface area (ECSA) analysis results for the trimetallic $\text{Au}_{\text{rod}}\text{-Pd}_{\text{shell}}\text{-Pt}_{\text{cluster}}$, bimetallic $\text{Au}_{\text{rod}}\text{-Pt}_{\text{cluster}}$ and monometallic JM-Pt (used as a reference), which have respective ECSA values (cm^2/mgPt)

of 1883.0, 1371.7 and 879. The potential utility of the trimetallic catalysts was shown in a hydrogen peroxide sensing protocol, which showed the catalyst to have a sensitivity of $604 \mu\text{A}/\text{mMcm}^2$ within a linear range of 0.0013–6.191 mM.

Keywords: trimetallic catalyst; Au core-shell; hydrogen peroxide sensing; nanoparticles; nanorods

1. Introduction

Catalysts incorporating metals with high catalytic ability, typically palladium and platinum, incur cost-penalties due to the scarcity of the active metal component; thus, structures that efficiently employ a minimal amount of material, while retaining high catalytic efficiency, are highly sought after. Core-shell structured catalysts, formulated to contain only small amounts of palladium and platinum, have been used in a range of catalytic applications [1].

The design history of catalytic materials shows a progression from simple mono-metallic catalysts, especially Pt, Pd and nano-dimensioned Au, to bimetallic structures: The addition of the second metal can not only help tailor sought after properties in terms of the particle's size, shape, and surface morphology, but can also heighten catalytic efficiency by the transfer of electron density from the underlying support metal into the surface catalytic architecture. In addition to the presence of a second metal the importance of catalyst-support interactions has also recently come to prominence [2–6].

The introduction of a third metal into the system should give the possibility of further tailoring the catalyst's performance. Some challenges and the outcome of interesting recent investigations are very briefly given below. Tompos *et al.*, 2007 [7], have used a combinatorial library design approach to synthesise of trimetallic Pt-Pd-Au/CeO₂ catalysts for total methane oxidation. It was shown that the addition of Pt and Au to palladium promoted the methane oxidation activity, as well as improved the long-term stability compared to the monometallic Pd catalyst. The authors also attribute enhanced activity to the formation of new active sites that adsorb methane more strongly than in the monometallic Pd catalyst. Yu *et al.*, 2013 [8], exploited a shape recovery phenomenon in Pt–Ni bimetallic nanocrystals attributable to defect effects. An intrinsic defect-dominated growth mechanism was shown to allow the site-selective nucleation of a third metal around the defects to design trimetallic Pt₃Ni@M core-shell structures (M = Au, Ag, Cu, Rh). Fang *et al.*, 2011 [1], designed Au-core Pd-shell Pt-cluster nanoparticles for enhanced electrocatalytic activity and showed using extremely small amounts of Pt and Pd unusually high activity for electrooxidation of formic acid in fuel cells. The optimized structures had only two atomic layers of Pd and a half-monolayer equivalent of Pt; interesting, it was found that further increasing the loading of Pd or Pt reduced catalytic activity, suggesting the presence of a synergistic effect among the three nano-structural components.

In this study a tri-metallic structure was sequentially fabricated with the initial stage being the deposition of Pd on Au rods to give a Au_{rod}-Pd_{shell} support for the later deposition of Pt: the ability to exploit high surface area to mass ratios of precious metals by using thin coating confers both enhanced activity/selectivity and considerable materials cost savings [4,5,9].

A practical evaluation of our trimetallic catalyst's properties, to enable comparison with those of Au_{rod}-Pt_{cluster}, Pt and catalysts [4,5,10–12], was made by comparative evaluation for hydrogen peroxide (H₂O₂) sensing. The accurate and reliable sensing of H₂O₂ is pivotal to a wide range of industrial, healthcare, and, more recently, anti-terrorism applications; some diverse examples being the bulk-scale bleaching of paper, aseptic packaging, bio-imaging, and the determination of clinically important analytes, such as glucose and uric acid. Despite its scientific and technological importance, the direct detection of hydrogen peroxide, resulting for example from the breakdown of glucose or urea by an oxidase enzyme, remains problematic, due to the absence of any UV absorbance or fluorescence activity. Thus, new approaches leading to the development of robust and sensitive H₂O₂ sensors remain an ongoing quest.

2. Experimental Section

2.1. Apparatus and Reagents

The supporting electrolyte, used for peroxide sensing, was phosphate buffer solution (PBS) containing 0.10 M Na₂HPO₄–NaH₂PO₄ + 0.10 M KCl (pH 7.4), all other chemicals were of analytical grade and used without further purification. Solutions were prepared and diluted using ultra-pure water (Millipore Milli Q system). Electrochemical experiments were performed using an Autolab PGSTAT302N electrochemical analyzer (AUTOLAB, USA) with a conventional three electrode cell. The working electrode was a glassy carbon electrode (GCE, diameter 5 mm). A silver/silver chloride (Ag/AgCl) and a platinum wire electrode were used as the reference and counter electrodes, respectively.

Powder X-ray diffraction (XRD) patterns were obtained on a diffractometer (RigakuDmax-B, Japan) using a Cu K_α source operating at 40 kV and 100 mA (scanning rate of 0.05 degs⁻¹ for 2θ values between 20 ° and 90 °). Transmission electron microscopy (TEM) examination was performed on a Philips Tecnai F20G2 FEI-TEM microscope operating with an accelerating voltage of 200 keV. The EDX measurements were performed with a JSM 6500 EDX analyzer. Specimens were prepared by ultrasonically suspending the catalyst powders in ethanol, applying the specimen to a copper grid and drying in air. Scanning electron microscopy (SEM) images were obtained at 5.0 keV on a Hitachi S-240 JOEL JSM-6500F field emission SEM. X-ray spectra were recorded at the National Synchrotron Radiation Research Center (NSRRC) of Taiwan, Beam Line 01C1, following the procedure described in detail in our previous publications [13,14].

The synthesis method employed a sequential strategy (see below). Initially, Au nanorods were prepared using existing methods. These were used as a platform for the deposition of a Pd thin-shell, which in turn served as the support for the Pt clusters.

2.2. Synthesis of Au Nanorods

Our synthesis is based on seed-mediated growth in aqueous solutions, which has been used widely for the preparation of Au nanostructures [15]. Briefly, the seed solution was prepared by rapidly injecting NaBH₄ (0.01 M, 0.6 mL) into a mixture of HAuCl₄ (64.5 uL 38.76 mM) and CTAB (3.75 mL, 0.20 M) and kept in a water bath, maintained at 25 °C, prior to use. To grow Au nanoparticles, a growth solution was prepared, comprising CTAB (0.2 M, 18.4 mL), HAuCl₄ 3H₂O (38.76 mM, 0.474 mL),

and AgNO_3 (0.368 mL, 0.01 M). To this solution was added ascorbic acid (0.2 M, 0.147 mL), then seed solution diluted 5 times with CTAB (0.1 M) to give a final volume of 100 μL was added into growth solution and left undisturbed overnight. The resulting nanocrystals were washed twice in the same solvent by centrifugation prior to use.

2.3. Synthesis of Au_{rod}-Pd Shell Structured Nanoparticles

In a typical synthesis the above aqueous Au_{rod} solution (0.6 mL) and 14.4 mM aqueous $\text{K}_2(\text{PdCl}_4)$ were added to DI water (41 mL). To this solution, 200 mM CTAB solution (8 mL) was added, after which ascorbic acid (200 mM, 80 μL) was rapidly injected with vigorous stirring during a period of 1 min. The solution was then heated in an oil bath at approximately 26 ± 2 °C 24 h, after which the particles were separated by centrifugation (8000 rpm for 6 min) to remove excess reagents [16].

2.4. Preparation of Au Rod-Pd Shell-Pt Cluster

To prepare the final catalytic structure DI water (42 mL), Au@Pd nanoparticles (1826 μL), K_2PtCl_4 (23.18 mM, 21.5 μL), and CTAB (200 mM, 49.8 mL) were mixed. To this mixture ascorbic acid (200 mM, 298 μL) was quickly added (within approximately 10 s) by injection. The resulting solution was heated in an oil bath 75 ± 2 °C for 15 min prior to being cooled in water. Centrifugation (5000 rpm/20 min/2 times) was used to isolate the final product.

2.5. Preparation of H₂O₂ Sensing Electrode

A glassy carbon electrode was polished, using Al_2O_3 powder, to remove surface impurities. The as-prepared catalyst was dispersed in 2 mL ultrapure water under sonication. Catalyst slurry, 15 μL , (transferred by pipette) was dropped onto the electrode's surface prior to oven drying.

2.6. Preparation of H₂O₂ Solution

H_2O_2 (4.280 mL, 11.68 M) was diluted with phosphate buffer solution (0.1 M, pH = 7.4) to a final volume of 50 mL to give H_2O_2 (1 M). The solution was stored at 4 °C prior to use.

2.7. H₂O₂ Sensing

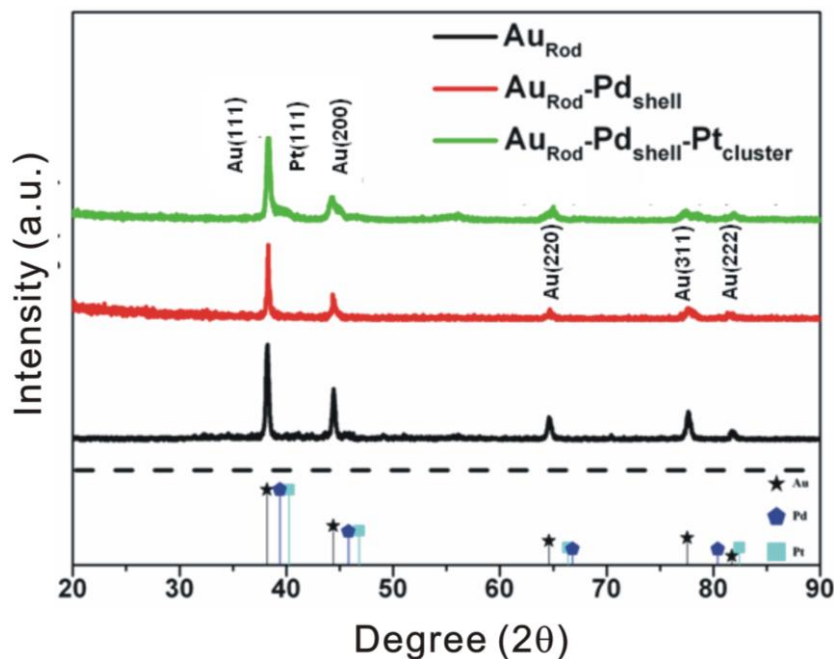
Amperometric measurements were conducted to investigate H_2O_2 catalytic sensitivity. The applied potential was set to 0.4 V, with aliquots of H_2O_2 , of known concentration, being added at 20 s intervals. A 5 s reaction time was allowed prior to measuring the variation in current response.

3. Results and Discussion

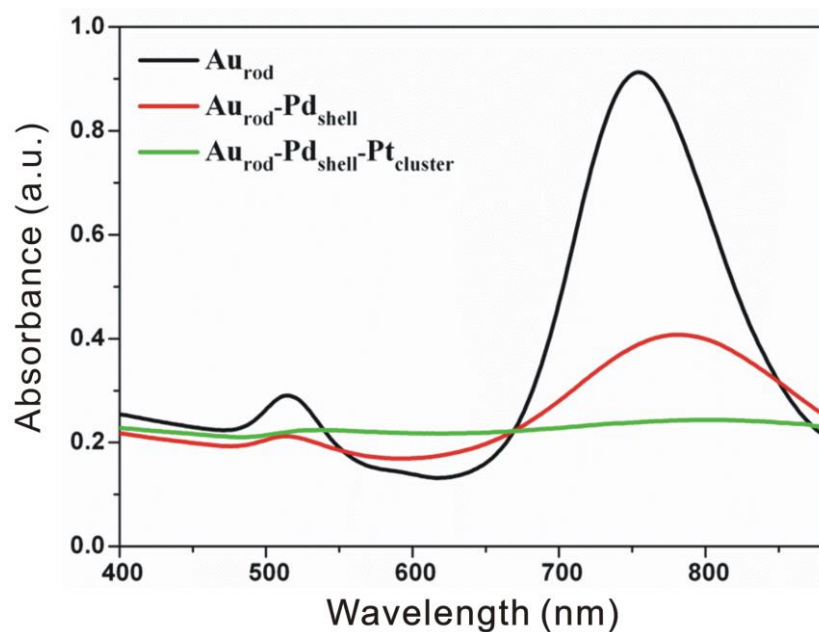
3.1. Characterization

The resulting nanoparticles were characterized by XRD, UV-vis, TEM, and XPS. Considering the XRD and UV spectra in conjunction with the TEM images clearly shows the formation of the composite catalyst, see Figures 1 and 2.

Figure 1. Material characterisation showing (a) XRD patterns and (b) UV spectra evolution as each additional added layer of the composite catalyst is added.



(a)

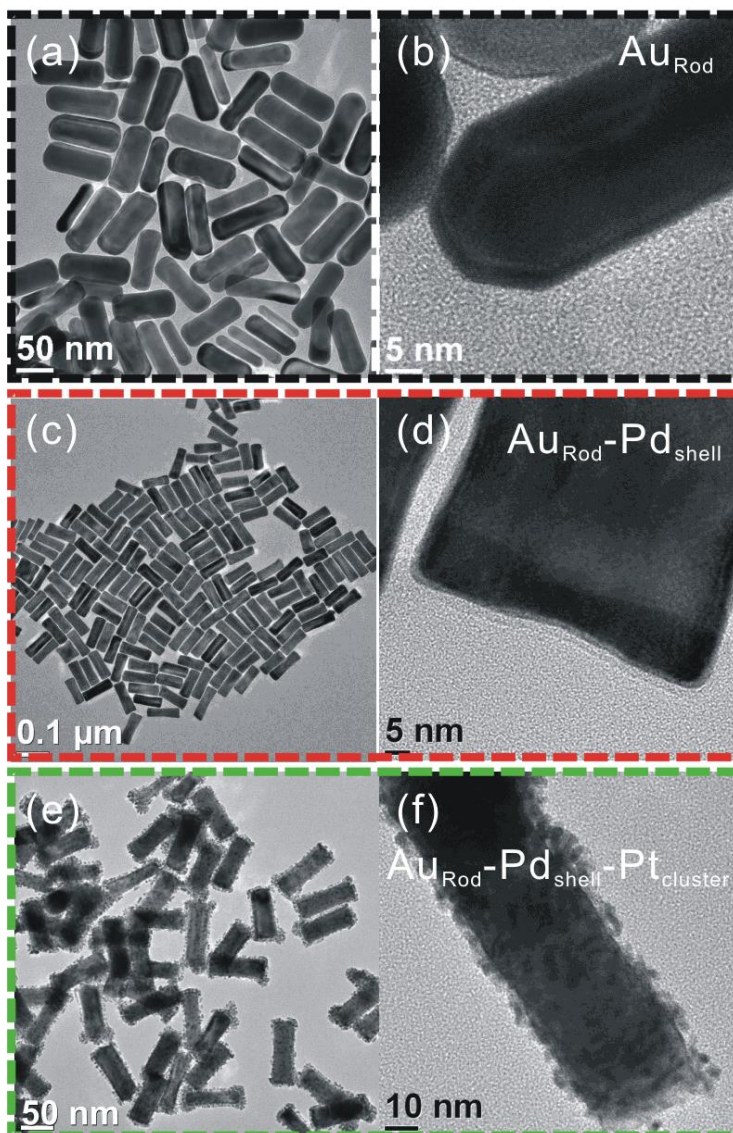


(b)

From the TEM images, we can see that the core-shell nanostructures consist of Au rod-like cores (distorted octagonal structures Figure 2a,b) with a Pd coating (rectangular structures Figure 2c,d), upon which a coating comprising Pt clusters is deposited, Figure 2e,f.

The XRD peak positions of the core-shell nanoparticles carrying the Pt clusters are similar to those of the core-shelled nanoparticles because the particle size of the Pt clusters is too small to give a distinct diffraction peak; however, the presence of Pt is confirmed by a Pt(111) shoulder which is apparent on the Au(111) peak.

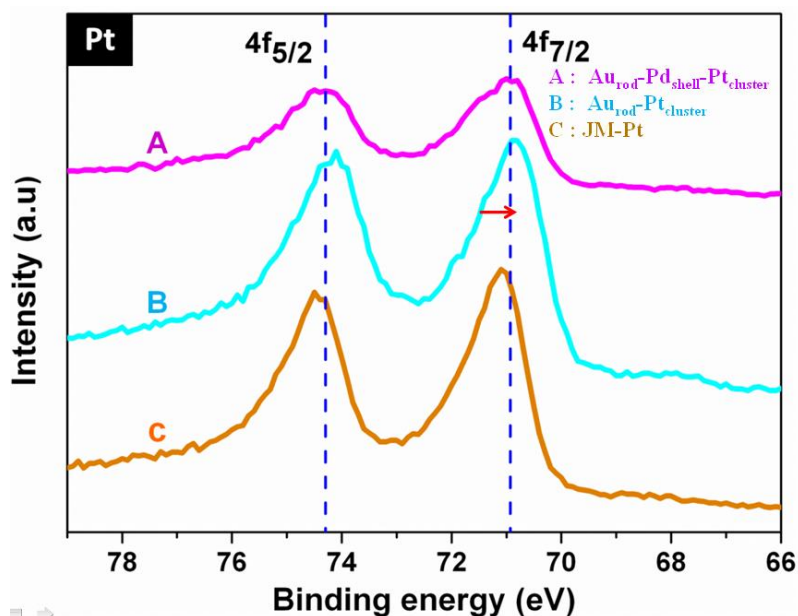
Figure 2. TEM images showing the stepwise formation of the catalyst: (a) Au rods; (b) Pd shell formed on the rods, and (c) after the formation of clustered Pt structures on the Pd shell.



The UV/Vis spectrum of the Au_{rods} displays the surface plasmon resonance peaks (centered at ~510 and 750 nm) associated with the Au core dipole resonance. These resonances are shown to be reduced in the Au_{rod}Pd_{shell} nanoaprticles (the resonance at ~510 disappearing almost entirely), and completely damped-out by the deposition of Pt, thereby indicating the formation of surface Pt deposition.

Catalytic efficiency is crucially dependent on the transfer of electron density from the underlying support metal into the surface catalytic architecture, e.g., from Au to Pt in Au_{rod}Pt_{cluster}, or Au_{rod}Pd_{shell}Pt_{cluster}, see Figure 3. The Pt 4f_{5/2} and 4f_{7/2} peaks for JM-Pt each show, as expected, only one component peak representative of the metal. However the spectra of Au_{rod}-Pt_{cluster} and especially Au_{rod}-Pd_{shell}-Pt_{cluster} show peak broadening, possibly due to the presence of multiple components, and a slight shift, due to charge transfer, towards lower binding energies. Similarly the number of unfilled *d* states (*h*_{Ts}), calculated with respect to a reference Pt foil (defined as 1.6) by a method previously published in the literature [13,14], showed the *d*-band vacancies of Pt for Au_{rod}-Pt_{cluster}, and the Au_{rod}Pd_{shell}Pt_{cluster} to decrease to 1.59043 and 1.5501, respectively.

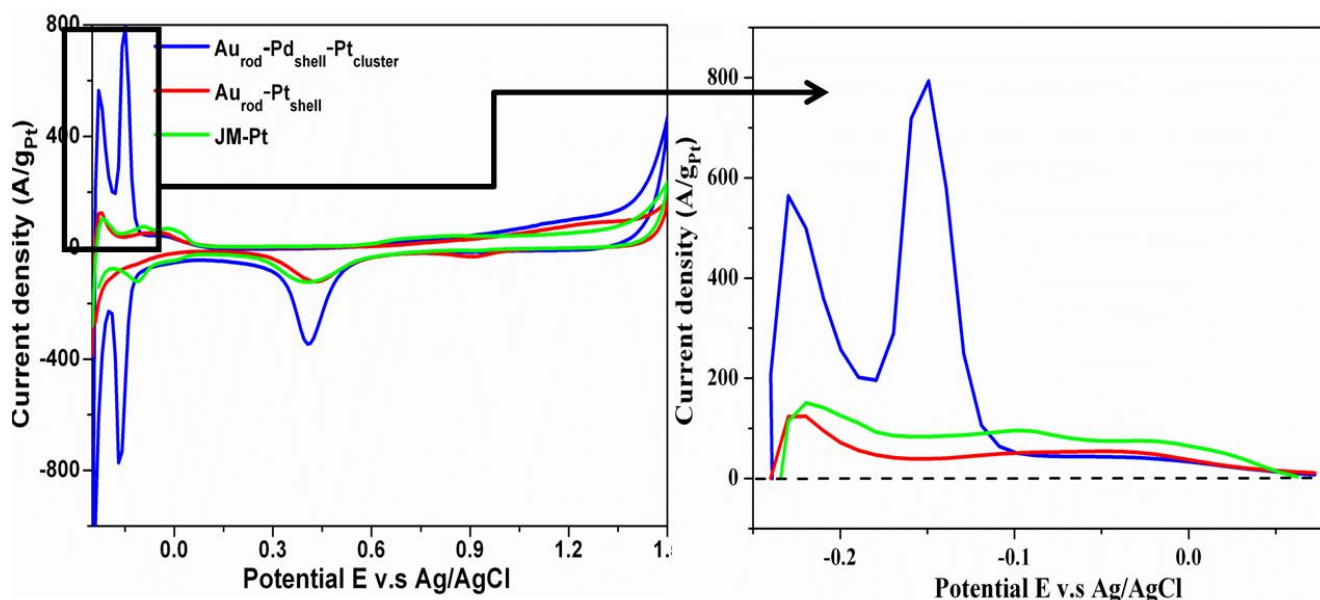
Figure 3. XPS spectra A: Au_{rod}-Pd_{shell}-Pt_{cluster}, B: Au_{rod}-Pt_{cluster}, C: JM-Pt.



3.2. Cyclic Voltammograms (CVs)

ECSA data derived from the final bimetallic core shell structure that carries the deposited Pt, shown in Figure 4 indicates the significantly higher specific ECSA of the Au_{rod}Pd_{shell}-Pt_{dendritic} nanostructures when compared to comparative data from Au_{rod}-Pt_{shell} and commercial JM-Pt. Figure 4b shows the ECSA profile from -0.25 V to 0.05 V and reflects, in a manner similar to the UV spectra, the transition in structure from a bimetallic shell structure to a Pt dominated surface structure. The calculated comparative hydrogen desorption areas are 55.9, 15.0, and 23.8 AV/gPt for Au_{rod}-Pd_{shell}-Pt_{cluster}, Au_{rod}-Pt_{cluster} and JM-Pt giving respective ECSA values of 1883.0, 1371.7 and 879 cm²/mgPt.

Figure 4. Comparative ECSA data from Au_{rod}Pd_{shell}-Pt_{clusters}, Au_{rod}-Pt_{shell} and commercial JM-Pt.



Cyclic voltammograms (CVs), made using a Ag/AgCl reference, of Au_{rod}/GCE (data not shown), Au-Pd/GCE and Au_{rod}-Pd-Pt/GCE, in 0.5 M H₂SO₄ solutions at a scan rate of 100 mVs⁻¹, revealed that the Au_{rod} nanoparticles exhibit a reduction peak at 0.90 V, this peak disappears on coating with Pd and a new reduction peak at approximately 0.38 V appears, while after coating with Pt, an electroactive Pt reduction peak at approximately 0.42 V appeared—allowing us to set the sensing potential to 0.4 V.

3.3. H₂O₂ Sensing Response

Figure 5a shows the response plotted as current density (μA/gram catalyst) of the Au_{rod}-Pd_{shell}-Pt_{cluster} assembly, together with similar data for AuPt_{shell} and JM-Pt catalysts (data normalized to a constant mass of Pt), to a stepwise challenge by H₂O₂; this is re-drawn in Figure 5b to show the response in terms of current density with respect to H₂O₂ concentration. The extracted data, tabulated in Table 1, show the sensitivity of the tri-metallic system to be ~2.6 times that of Pt clusters formed as Au_{rod}-Pt_{cluster} structures and ~1.6 times that of commercially available JM-Pt.

Figure 5. (a) shows current density response to the stepwise addition of H₂O₂, while (b) shows the data plotted as current density versus H₂O₂ concentration.

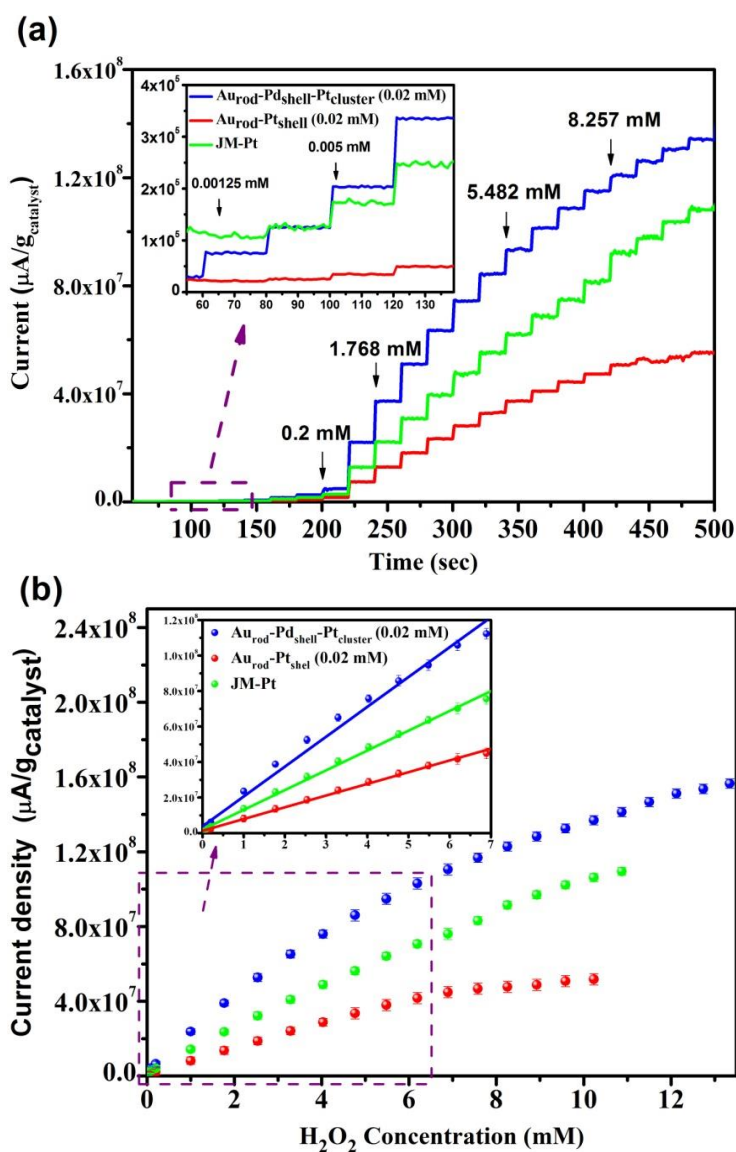


Table 1. Relationship of catalytic structures to hydrogen peroxide sensing.

| Applied potential (0.4 V) vs. Ag/AgCl | Linear range (μM) | H_2O_2 sensitivity ($\mu\text{A}/\mu\text{M}\times\text{g}_{\text{cat}}$) | R^2 |
|--|--------------------------------|--|--------------|
| $\text{Au}_{\text{rod}}\text{-Pd}_{\text{shell}}\text{-Pt}_{\text{cluster}}$ | 0.00125–6.191 | 17,721 | 0.99364 |
| $\text{Au}_{\text{rod}}\text{-Pt}_{\text{cluster}}$ | 0.005–5.482 | 6612 | 0.99765 |
| JM-Pt | 0.005–6.191 | 11,144 | 0.9978 |

Comparison of the measured H_2O_2 sensing data with that previously published shows the linear detection range to extend to ultra-low concentrations. The upper detection limit within the linear detection range exceeds that of most recently published studies. In a recent study a linear detection range of 0.012–14 mM was reported [4]; however, the associated sensitivity was $393 \mu\text{A}/\text{mMcm}^2$ in contrast with the $604 \mu\text{A}/\text{mMcm}^2$ determined in this study.

4. Conclusions

The evident synergy resulting from the use of three metals is clearly shown by the significantly higher specific ECSA of the $\text{Au}_{\text{rod}}\text{Pd}_{\text{shell}}\text{-Pt}_{\text{dendritic}}$ nanostructures when compared to comparative data from $\text{Au}_{\text{rod}}\text{-Pt}_{\text{shell}}$ and commercial JM-Pt. This is reflected in our H_2O_2 sensing response data (which additionally exhibited a slightly extended linear range) that showed the sensitivity of our fabricated mini-sensor, made with the tri-metallic construct, to be 2.68 times greater than an electrode made as a simple $\text{Au}_{\text{rod}}\text{-Pt}_{\text{cluster}}$ and 1.59 times greater than one fabricated with JM-Pt (all under similar conditions).

The core-shell trimetallic catalysts retain a high catalytic ability while using only small amounts of the precious metals, especially palladium and platinum; each sensor being fabricated with a nanoparticle solution (15 μL) comprising a total of 6.7 μg of the active metals (Au 4.9 μg , Pd 1.07 μg and Pt 0.73 μg).

This study, highlighting the use of an optimized tri-metallic rather than a bimetallic structure, serves to highlight the possibility of using tailored combinations of precious catalytic materials, in new morphologies, to address the challenges imposed by the need to make ever more active catalysts using lower amounts of precious materials.

Acknowledgments

The financial supports from the Ministry of Science and Technology (MOST) (103-3113-E-011-001, 101-3113-E-011-002, 101-2923-E-011-001-MY3, 100-2221-E-011-105-MY3), the Ministry of Economic Affairs (MOEA) (101-EC-17-A-08-S1-183), and the Top University Projects of Ministry of Education (MOE) (100H451401), as well as the facilities supports from the National Taiwan University of Science and Technology (NTUST), and National Synchrotron Radiation Research Centre (NSRRC) are acknowledged.

Author Contributions

B.-J. Hwang conceived the project and designed the experiments. S.-I. Cheng, C.-J. Pan and K.-J. Chen performed material synthesis, structural characterization and electrochemical measurements. Y.-W. Yang, C.-H. Wang and C.-J. Pan performed the XPS and XAS measurement and analysis.

J. Rick, H.-L. Chou, W.-N. Su and B.-J. Hwang analyzed the data. J. Rick, H.-L. Chou, C.C. Liu and B.-J. Hwang co-wrote the paper. All authors discussed the results and commented on the manuscript.

Conflicts of Interest

The authors declare no conflict of interest.

References

1. Fang, P.P.; Duan, S.; Lin, X.D.; Anema, J.R.; Li, J.F.; Buriez, O.; Ding, Y.; Fan, F.R.; Wu, D.Y.; Ren, B.; Wang, Z.L.; Amatore, C.; Tian, Z.Q. Tailoring Au-core Pd-shell Pt-cluster nanoparticles for enhanced electrocatalytic activity. *Chem. Sci.* **2011**, *2*, 531–539.
2. Antolini, E. Composite materials: An emerging class of fuel cell catalyst supports. *Appl. Catal. B* **2010**, *100*, 413–426.
3. Campbell, C.T. Electronic perturbations. *Nat. Chem.* **2012**, *4*, 597–598.
4. Chen, K.L.; Lee, C.F.; Rick, J.; Wang, S.H.; Liu, C.C.; Hwang, B.J. Fabrication and application of amperometric glucose biosensor based on a novel PtPd bimetallic nanoparticle decorated multi-walled carbon nanotube catalyst. *Biosens. Bioelectron.* **2012**, *33*, 75–81.
5. Chen, K.L.; Pillai, C.; Rick, J.; Pan, C.J.; Wang, S.H.; Liu, C.C.; Hwang, B.J. Bimetallic PtM (M = Pd, Ir) nanoparticle decorated multi-walled carbon nanotube enzyme-free, mediator-less amperometric sensor for H₂O₂. *Biosens. Bioelectron.* **2012**, *33*, 120–127.
6. Chen, C.H.; Sarma, L.S.; Wang, G.R.; Chen, J.M.; Shih, S.C.; Tang, M.T.; Liu, D.G.; Lee, J.F.; Chen, J.M.; Hwang, B.J. Formation of bimetallic Ag-Pd nanoclusters via the reaction between Ag nanoclusters and Pd²⁺ ions. *J. Phys. Chem. B* **2006**, *110*, 10287–10295.
7. Tompos, A.; Margitfalvia, J.L.; Hegedusa, M.; Szegedia, Á.; Fierrob, J.L.G.; Rojasb, S. Characterization of trimetallic Pt-Pd-Au/CeO₂ catalysts combinatorial designed for methane total oxidation. *Comb. Chem. High Throughput Screen.* **2007**, *10*, 71–82.
8. Wu, Y.; Wang, D.; Chen, X.; Zhou, G.; Yu, R.; Li, Y. Defect-dominated shape recovery of nanocrystals: A new strategy for trimetallic catalysts. *J. Am. Chem. Soc.* **2013**, *135*, 12220–12223.
9. Song, H.M.; Anjum, D.H.; Sougrat, R.; Hedhili, M.N.; Khashab, N.M. Hollow Au@Pd and Au@Pt core-shell nanoparticles as electrocatalysts for ethanol oxidation reactions. *J. Mater. Chem.* **2012**, *22*, 25003–25010.
10. Zou, Y.; Xiang, C.; Sun, L.X.; Xu, F. Glucose biosensor based on electrodeposition of platinum nanoparticles onto carbon nanotubes and immobilizing enzyme with chitosan-SiO₂ sol-gel. *Biosens. Bioelectron.* **2008**, *23*, 1010–1016.
11. Debiemme, C. A very thin overoxidized polypyrrole membrane as coating for fast time response and selective H₂O₂ amperometric sensor. *Biosens. Bioelectron.* **2010**, *25*, 2454–2457.
12. Xu, C.; Liu, Y.; Su, F.; Liu, A.; Qiu, H. Nanoporous PtAg and PtCu alloys with hollow ligaments for enhanced electrocatalysis and glucose biosensing. *Biosens. Bioelectron.* **2011**, *27*, 160–166.
13. Hwang, B.J.; Kumar, S.M.S.; Chen, C.H.; Chang, R.W.; Liu, D.G.; Lee, J.F. Size and alloying extent dependent physicochemical properties of Pt-Ag/C nanoparticles synthesized by the ethylene glycol method. *J. Phys. Chem. C* **2008**, *112*, 2370–2377.

14. Lai, F.J.; Sarma, L.S.; Chou, H.L.; Liu, D.G.; Hsieh, C.A.; Lee, J.F.; Hwang, B.J. Architecture of bimetallic Pt_xCo_{1-x} electrocatalysts for oxygen reduction reaction as investigated by X-ray absorption spectroscopy. *J. Phys. Chem. C* **2009**, *113*, 12674–12681.
15. Ming, L.; Xi, X.; Liu, J. Electrochemically platinized carbon paste enzyme electrodes: A new design of amperometric glucose biosensors. *Biotechnol. Lett.* **2006**, *28*, 1341–1345.
16. Kim, Y.; Hong, J.W.; Lee, Y.W.; Kim, M.; Kim, D.; Yun, W.S.; Han, S.W. Synthesis of AuPt heteronanostructures with enhanced electrocatalytic activity toward oxygen reduction. *Angew. Chem.* **2010**, *49*, 10197–10201.

© 2014 by the authors; licensee MDPI, Basel, Switzerland. This article is an open access article distributed under the terms and conditions of the Creative Commons Attribution license (<http://creativecommons.org/licenses/by/4.0/>).